Representation of microstructural features and magnetic anisotropy of electrical steels in an energy-based vector hysteresis model

Kevin Jacques, Simon Steentjes, François Henrotte, Christophe Geuzaine, and Kay Hameyer

Citation: AIP Advances **8**, 047602 (2018);
View online: https://doi.org/10.1063/1.4994199
View Table of Contents: http://aip.scitation.org/toc/adv/8/4
Published by the American Institute of Physics

Representation of microstructural features and magnetic anisotropy of electrical steels in an energy-based vector hysteresis model

Kevin Jacques,[1,2,a] Simon Steentjes,[3,b] François Henrotte,[1] Christophe Geuzaine,[1] and Kay Hameyer[3]
[1]*Institute Montefiore - ACE - Université de Liège, B-4000 Liège, Belgium*
[2]*BEAMS Department - Université Libre de Bruxelles, B-1050 Bruxelles, Belgium*
[3]*Institute of Electrical Machines - RWTH Aachen University, D-52056 Aachen, Germany*

(Received 4 July 2017; accepted 9 August 2017; published online 13 October 2017)

This paper demonstrates how the statistical distribution of pinning fields in a ferromagnetic material can be identified systematically from standard magnetic measurements, Epstein frame or Single Sheet Tester (SST). The correlation between the pinning field distribution and microstructural parameters of the material is then analyzed. https://doi.org/10.1063/1.4994199

I. INTRODUCTION

Ferromagnetic materials are ubiquitous in industrial and household applications. They are characterized by a nonlinear and dissipative behavior determined by a rich and complex microstructure involving grains, Weiss magnetic domains, Bloch walls and magnetic inhomogeneities or defects, see e.g. Refs. 1 and 2. Designing and optimizing devices with ferromagnetic parts requires thus, among others, a consistent hysteresis model whose parameters can be identified from easily available measurement data.

There exists only one dissipation mechanism in ferromagnetic materials: Joule losses associated with the local variation of the magnetic polarization $\mathbf{J}$. More particularly, the magnetic hysteresis is associated with Joule losses occurring when the applied magnetic field varies in quasi-static conditions, i.e. at vanishing frequency.

Schematically, losses in quasi-static regime are due to the existence of local minima (energy wells) in the energy functional of the microscopic magnetic moments in the material. As the applied magnetic field changes, the magnetic state does not change significantly in a first time because microscopic moments are trapped in some energy well. When a field threshold is reached, the magnetic moment can escape the energy well. The magnetic state then jumps to another state with a sudden local rotation of some magnetic moments that induces local eddy currents and losses, so that, after damping, a new stable state is reached. At the macroscopic scale, a jerky evolution of the magnetic polarization of the sample is observed, which is called Barkhausen effect.

With this picture in mind, we can characterize the ferromagnetic material, from a macroscopic point of view, as a statistical distribution of energy wells of various depths. The depths of the well is a potential barrier, i.e., the amount of energy needed to escape the well. The potential barriers explaining hysteresis in ferromagnetic materials are to ascribe to (*i*) the anisotropy of crystallites (grains) and the existence of easy magnetization directions, and (*ii*) the pinning of Bloch walls by defects. The two types of barrier can not be distinguished from a macroscopic analysis and are therefore not distinguished by our model. Moreover, as the magnetic moments have a constant module,

[a]Electronic mail: Kevin.Jacques@doct.ulg.ac.be
[b]Electronic mail: Simon.Steentjes@iem.rwth-aachen.de

the potential barrier can also be expressed as a magnetic field κ, abstractly called pinning field. We show in this paper that the macroscopic coercivity of ferromagnetic materials can be characterized by a pinning field distribution function $\omega(\kappa)$, which can be systematically identified from standard magnetic measurements.

The energy-based hysteresis model[3–6,12] relies on a fundamental analogy between the pinning fields κ and a dissipative dry friction force. This paper demonstrates how, based on this analogy, the pinning field probability density $\omega(\kappa)$ mentioned above can be identified systematically from standard magnetic measurements, obtained with either an Epstein frame or a Single Sheet Tester (SST). The identified pinning field distribution is first of all a very informative characteristic, giving insight into the microstructure of the material. It allows also classifying and comparing different steel grades with each other on an objective basis.

The microscopic nature of the pinning field is accounted for in the macroscopic hysteresis model by applying a two-scale approach. The ferromagnetic material sample is decomposed into independent abstract regions, all subjected to the same macroscopic magnetic field $\mathbf{h}$, but characterized individually by a particular value of the pinning field κ. The identification of the pinning field probability density $\omega(\kappa)$ is a major step for the representation of ferromagnetic materials in a finite element model for instance, as it contains the information needed to determine straightforwardly the free parameters of the energy-based hysteresis model.

II. ENERGY-BASED HYSTERESIS MODEL

The hysteresis model[3] is based on the the conservation of energy

$$\dot{\Psi} = \mathbf{h} \cdot \dot{\mathbf{b}} - D \tag{1}$$

where Ψ is the magnetic energy density of the material, $\mathbf{h} \cdot \dot{\mathbf{b}}$ the magnetic work, and D a dissipation function representing magnetic hysteresis. A dot above a symbol denotes a time derivative. The magnetic energy density Φ contains an internal energy term u related to material magnetic moments and an empty space term,

$$\Psi = u + \mu_0 \frac{|\mathbf{h}|^2}{2}. \tag{2}$$

The empty space contribution plays however no role in the identification problem and can be eliminated by rewriting (1) as

$$\dot{u} = \mathbf{h} \cdot \dot{\mathbf{J}} - D \quad , \quad \mathbf{J} = \mathbf{b} - \mu_0 \mathbf{h}. \tag{3}$$

The internal energy is an explicit function of the magnetic polarization $\mathbf{J}$, $u = u(\mathbf{J})$, and its time derivative writes

$$\dot{u} = \mathbf{h}_r \cdot \dot{\mathbf{J}} \quad \text{with} \quad \mathbf{h}_r := \partial_{\mathbf{J}} u. \tag{4}$$

The field $\mathbf{h}_r$ is called *reversible magnetic field*, because the magnetic work it delivers under a variation of the magnetic polarization, is fully converted into internal energy. If we assume that the internal energy functional u is smooth and convex, there is a 1-1 relationship between $\mathbf{h}_r$ and $\mathbf{J}$, which we shall represent with the anhysteretic magnetic characteristic of the material

$$\mathbf{J} = \mathbf{J}_{\text{an}}(\mathbf{h}_r). \tag{5}$$

Note that the function $\mathbf{J}_{\text{an}} : \mathbf{h}_r \mapsto \mathbf{J}$ is just a handy notation for the inverse of the function $\partial_{\mathbf{J}} u : \mathbf{J} \mapsto \mathbf{h}_r$.

Magnetic hysteresis losses can be interpreted in terms of the mechanical analogy depicted in Fig. 1 (left).[4,5] In this representation, the applied force corresponds to the applied magnetic field $\mathbf{h}$ while the elongation corresponds to the magnetic polarization $\mathbf{J}$. The applied magnetic field $\mathbf{h}$ is thus decomposed into a reversible part $\mathbf{h}_r$ and an irreversible part $\mathbf{h}_{irr}$, acting respectively as spring force and friction force. The friction slider unlocks when the applied field exceeds the pinning field threshold κ, allowing then the spring to elongate, and thus to store magnetic energy.

The dissipation functional associated with dry friction writes

$$D = \kappa |\dot{\mathbf{J}}| := \mathbf{h}_{irr} \cdot \dot{\mathbf{J}} \tag{6}$$

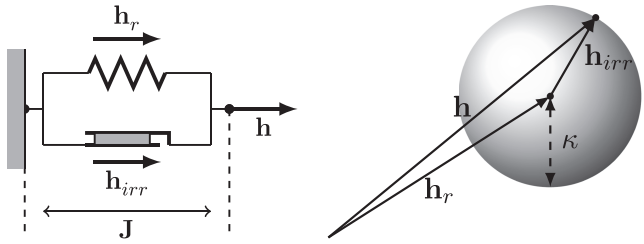

FIG. 1. Mechanical analogy (left) and pictorial representation (right) of the energy-based model.

in terms of the field $\mathbf{h}_{irr}$, which is called *irreversible magnetic field*, because the associated magnetic work is integrally dissipated. Because the functional (6) is not differentiable in $\dot{\mathbf{J}} = 0$, one is not allowed to simply write $\mathbf{h}_{irr} = \partial_{\dot{\mathbf{J}}} D$. The functional is however convex and convex analysis can be invoked to define $\mathbf{h}_{irr}$, not as a single-valued gradient, but as a set

$$\mathbf{h}_{irr} \in \left\{ \mathbf{h}_{irr}, |\mathbf{h}_{irr}| \leq \kappa \text{ if } \dot{\mathbf{J}} = 0, \mathbf{h}_{irr} = \kappa \frac{\dot{\mathbf{J}}}{|\dot{\mathbf{J}}|} \text{ otherwise} \right\}, \tag{7}$$

called the *subgradient* of the functional D.

With these definitions, the energy conservation (1) writes

$$(\mathbf{h} - \mathbf{h}_r - \mathbf{h}_{irr}) \cdot \dot{\mathbf{J}} = 0, \tag{8}$$

and, as it must hold for any $\dot{\mathbf{J}}$, one has the equilibrium equation

$$\mathbf{h} - \mathbf{h}_r - \mathbf{h}_{irr} = 0, \tag{9}$$

which is the fundamental evolution relation of the energy-based hysteresis model. Now, as the applied magnetic field $\mathbf{h}$ evolves in time, two cases are to be considered. As long as the condition

$$|\mathbf{h} - \mathbf{h}_r| \leq \kappa \tag{10}$$

is verified, there is a $\mathbf{h}_{irr}$ in the set (7) that verifies (9), and $\mathbf{h}_r$ remains unchanged, which means that the magnetic polarization (5) is also unchanged. A change in the applied magnetic field $\mathbf{h}$ yields in this case no change in the magnetic polarization. This is the typical behavior of dry friction. If now $\mathbf{h}(t)$ changes in such a way that the condition (10) is no longer verified, the definition of the subgradient gives

$$\mathbf{h} - \mathbf{h}_r = \kappa \frac{\dot{\mathbf{J}}_{\text{an}}(\mathbf{h}_r)}{|\dot{\mathbf{J}}_{\text{an}}(\mathbf{h}_r)|}, \tag{11}$$

which is a nonlinear differential relationship to solve for $\mathbf{h}_r$ at each instant of time. It has a unique solution, which we note $\mathbf{h}_r(t) = U(\mathbf{h}(t))$ in terms of the so-called update rule U of the model. Different methods, which need not be detailed here, can be used to solve (11), with various degrees of accuracy.

Fig. 1 (right) provides a visual representation of the update rule. The sphere of radius κ centered in $\mathbf{h}_r$ is the representation of the subgradient (7). Equation (10) imposes that the tip of the applied magnetic field vector $\mathbf{h}$ is either inside of the sphere or on its surface. As long as the tip of the applied magnetic field vector $\mathbf{h}$ is inside the sphere, (10) is fulfilled and the sphere remains fixed, which means that both $\mathbf{h}_r$ and the magnetic polarization $\mathbf{J}$ are constant. If now the magnetic field vector $\mathbf{h}$ tends to stick out of the sphere, the sphere has to shift to accommodate condition (10), i.e., the sphere moves according to the update rule $\mathbf{h}_r(t) = U(\mathbf{h}(t))$. In this situation, the magnetization changes, $\dot{\mathbf{J}} \neq 0$. Fig. 2 shows this evolution for the case of a unidirectional variation of the applied magnetic field $\mathbf{h}$, both in the $\mathbf{h} - \mathbf{h}_r$ and in the $\mathbf{h} - \mathbf{J}$ planes. The evolution writes $h = h_r \pm \kappa$ along the ascending ($\dot{J} > 0$) and descending ($\dot{J} < 0$) branches, respectively.

The notion of subgradient implies that there exists no 1-1 relationship between $\mathbf{h}(t)$ and $\mathbf{h}_{irr}(t)$, and hence between $\mathbf{h}(t)$ and $\mathbf{h}_r(t)$. This non-univocity is the fundamental justification why the response of a hysteretic material depends not only on the applied field $\mathbf{h}(t)$, but also on the history. The vector $\mathbf{h}_r$ plays the role of history parameter in this model.

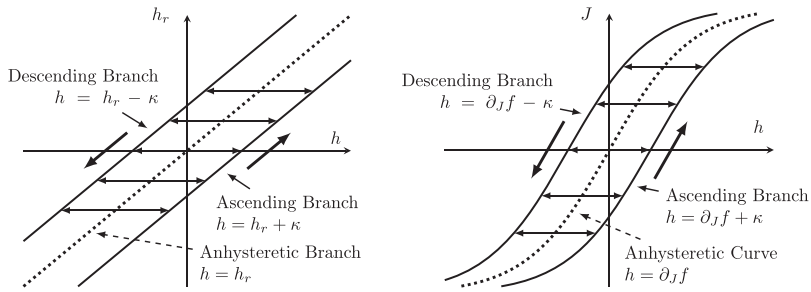

FIG. 2. Evolution of the reversible magnetic field h_r (left) and magnetic polarization J (right) as a function an unidirectional applied magnetic field h.

III. TWO-SCALE MODEL

Minor loops and the initial magnetization curve (virgin curve) display unrealistic horizontal transition lines in Fig. 2. This is due to the fact that all magnetic moments making up the material were attributed the same pinning field value κ. This is not the case in real ferromagnetic materials, which are rather characterized by a statistical distribution of pinning fields.[1,3,7,8]

The idea of the multi-cell model consists in saying that the material, which is homogeneous at the macroscopic scale, is composed of heterogeneous microscopic abstract regions characterized by a fixed value of κ. This is a kind of multi-scale model. The statistical weight of each microscopic region is given by a probability density $\omega(\kappa)$, $\int_0^\infty \omega(\kappa)\,\mathrm{d}\,\kappa = 1$. It is also assumed that the microscopic regions are independent of each other, and that the single-cell model described in the previous section is applicable in each of them. In particular, the evolution of the reversible magnetic field $h_r^\star(\kappa)$ in the microscopic region characterized by the pinning field κ is determined by the equations

$$|\mathbf{h}^\star(\kappa) - \mathbf{h}_r^\star(\kappa)| \le \kappa \tag{12}$$

and

$$\mathbf{h}^\star(\kappa) - \mathbf{h}_r^\star(\kappa) = \kappa \frac{\dot{\mathbf{J}}_{\mathrm{an}}(\mathbf{h}_r^\star(\kappa))}{|\dot{\mathbf{J}}_{\mathrm{an}}(\mathbf{h}_r^\star(\kappa))|}, \tag{13}$$

where the star indicates a quantity related to an abstract microscopic region. With these equations, the reversible magnetic field $\mathbf{h}_r^\star(\kappa)$ can be evaluated independently in each individual region, and the macroscopic reversible magnetic field $\mathbf{h}_r$ is evaluated taking into account the weighting of the different regions. All microscopic regions being subject to the same applied magnetic field $\mathbf{h}$, the localization and homogenization relationships of this multi-scale formulation read

$$\mathbf{h}^\star(\kappa) = \mathbf{h}, \quad \mathbf{h}_r = \int_0^\infty \omega(\kappa)\,\mathbf{h}_r^\star(\kappa)\,d\kappa. \tag{14}$$

Once the macroscopic reversible magnetic field $\mathbf{h}_r$ is known, the magnetic flux density and the terms of the energy balance are evaluated as follows

$$\mathbf{b} = \mathbf{J}_{\mathrm{an}}(\mathbf{h}_r) + \mu_0\mathbf{h}, \quad D = \mathbf{h}\cdot\dot{\mathbf{b}} - \dot{u}(\mathbf{J}_{\mathrm{an}}(\mathbf{h}_r)). \tag{15}$$

IV. IDENTIFICATION OF THE PINNING FIELD PROBABILITY DENSITY $\omega(\kappa)$

In this model, the memory of the material is represented at each instant of time by the distribution of the reversible magnetic field $\mathbf{h}_r^\star(\kappa)$, the demagnetized state (wiped-out memory state) being the state with $\mathbf{h}^\star(\kappa) = 0, \forall\kappa$. It is remarkable that the pinning field probability density $\omega(\kappa)$ can be identified from standard Epstein (or SST) measurements. As the loading is always unidirectional in such measurements, we shall work throughout this section with the modulus of the field $h = |\mathbf{h}|$ and $h_r^\star = |\mathbf{h}_r^\star|$.

Starting from the demagnetized state, a unidirectional magnetic loading until $h = h_{\mathrm{A}}$ is first applied to the material. The microscopic regions whose magnetic state is modified by this loading

are those for which $\kappa < h_A$ and one has for them, at the end of the loading, $h_r^\star(\kappa) = h_A - \kappa$, the other $h_r^\star(\kappa)$ remaining zero. The homogenized macroscopic reversible field is then

$$h_r(0 \to h_A) = \int_0^\infty \max(h_A - \kappa, 0)\, \omega(\kappa)\, d\kappa = F(h_A)$$

with the definition of an auxiliary function

$$F(h) := \int_0^h \omega(\kappa)\, (h - \kappa)\, \mathrm{d}\kappa, \tag{16}$$

whose first and second derivatives are respectively

$$\partial_h F(h) = \int_0^h \omega(\kappa)\, \mathrm{d}\kappa, \quad \partial_h^2 F(h) = \omega(h). \tag{17}$$

Starting over from this state, the material is now unloaded until the magnetic field reaches $h_B < h_A$, always in the same direction. The microscopic regions involved in the unloading are those such that $h_B + \kappa < h_A - \kappa$, i.e. $\kappa < (h_A - h_B)/2$. One has then

$$\begin{aligned} h_r(0 \to h_A \to h_B) &= \int_0^\infty \min(h_B + \kappa, \max(h_A - \kappa, 0))\, d\kappa \\ &= \int_0^{\frac{h_A - h_B}{2}} \omega(\kappa)(h_B + \kappa)\, d\kappa + \int_{\frac{h_A - h_B}{2}}^{h_A} \omega(\kappa)(h_A - \kappa)\, d\kappa \\ &= \int_0^{h_A} \omega(\kappa)(h_A - \kappa)\, d\kappa - 2\int_0^{\frac{h_A - h_B}{2}} \omega(\kappa)\Big(\frac{h_A - h_B}{2} - \kappa\Big)\, d\kappa \\ &= F(h_A) - 2F(\frac{h_A - h_B}{2}). \end{aligned}$$

The auxiliary function F, whose second derivative is the sought distribution $\omega(\kappa)$, plays a central role. If we can identify F, ω is also identified in principle.

The *virgin curve* of the material (first magnetization curve) is also simply the composition of the anhysteretic curve with F:

$$J_{\text{virgin}}(h) = J_{\text{an}}\Big(h_r(0 \to h)\Big) = J_{\text{an}}\Big(F(h)\Big). \tag{18}$$

This relationship could serve as a basis for the identification of F. However, the anhysteretic curve is not part of standard magnetic measurement setups (Epstein or SST). Therefore, an identification strategy independent of J_{an} is preferable. To find one, it is first noted that the coercive field $h_c(h)$ of a hysteresis loop of magnitude h is characterized by

$$J_{\text{an}}\Big(h_r(0 \to h \to -h_c(h))\Big) = 0, \tag{19}$$

which implies

$$F(h) - 2F\Big(\frac{h + h_c(h)}{2}\Big) = 0. \tag{20}$$

The coercive field characteristic $h_c(h)$ is obtained from the measurement of a series of symmetric hysteresis loops of increasing amplitude. Figure 3 depicts the measured $h_c(h)$ characteristics for five different non-oriented electrical steel grades. Remarkably, the $h_c(h)$ characteristics of a material contains enough information to completely identify the function F, and hence the pinning field probability density $\omega(\kappa)$ of the material.

From a mathematical point of view, the coercive field characteristic has the following properties:

(i) $h_c(0) = 0$,
(ii) $\exists h_s, h_c(h) = h_{c,\max}\ \forall h > h_s$,
(iii) $h_c(h) < h$.

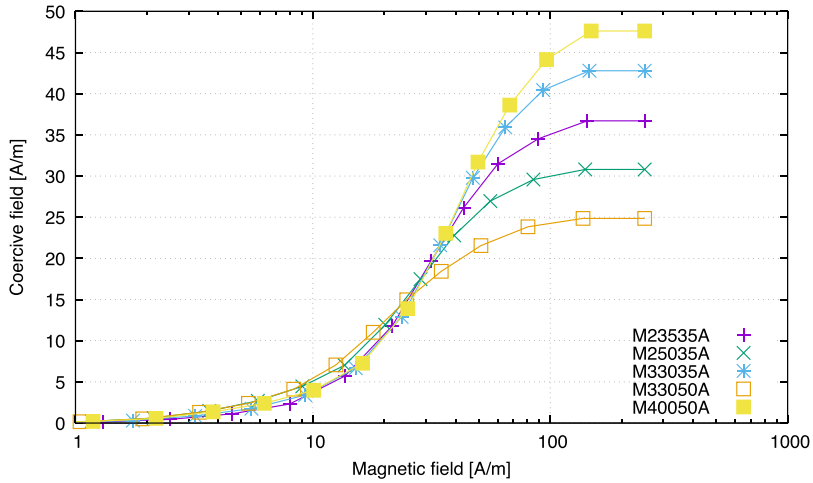

FIG. 3. Coercive field $h_c(h)$ of symmetrical hysteresis loops measured for five different non-oriented electrical steel grades.

Property (i) tells indeed that $F(0) = 0$. From (ii), one sees that $F(h) = h - h_{c,\max}, \forall h > h_s$. Finally, (iii) implies that the series defined by

$$x^n = (x^{n-1} + h_c(x^{n-1}))/2 < x^{n-1} \tag{21}$$

is strictly decreasing. Starting from an arbitrary initial value $x^0 > h_s$, for which it is known that $F(x^0) = x^0 - h_{c,\max}$, the value of F for all subsequent terms of the series is recursively given by $F(x^n) = F(x^{n-1})/2$. Clearly, the series converges towards $F(0) = 0$.

The coercive field characteristic for the material M235-35A and the series $F(x^n)$ are depicted in Fig. 4. The coercive field characteristic is interpolated linearly in the measurement range $[h_{\min}, h_{\max}]$, and it is extrapolated as follows

$$h_c(h) = h_{c,\max} \quad \text{if} \quad h > h_{\max}$$
$$h_c(h) = h_{c,\min}\left(\frac{h}{h_{\min}}\right)^2 \quad \text{if} \quad h < h_{\min}$$

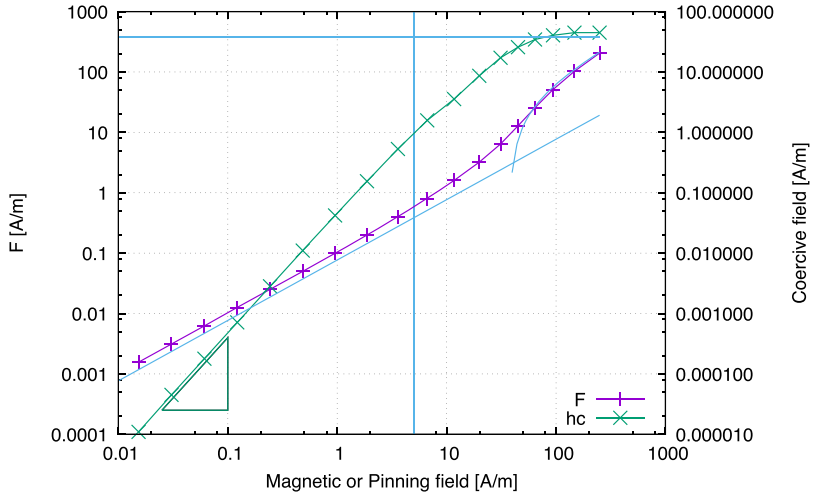

FIG. 4. Coercive field characteristic and F function for the steel grade M235-35A, in logarithmic scale. The asymptotic behavior is indicated with solid lines for both curves. The vertical line indicates the lower bound of the measurement range.

for field values outside the measurement range. The quadratic extrapolation at low fields is the one that has been observed to give the best results. One sees in Fig. 4 that it prolongates reasonably the general shape of the characteristic, which was measured from $h_{\min} = 5.11$ A/m.

With a properly inter- and extrapolated $h_c(h)$ characteristic, the iteration (21) can be carried out. As it is a geometric progression, the points of the series are almost equidistant in a logarithmic scale. One sees that the function $F(h)$ is smooth, and its asymptotic behavior is well defined

$$F(h) = h - h_{c,\max} \quad \text{if} \quad h > h_{\max}$$
$$F(h) = \alpha h \quad \text{if} \quad h < h_{\min}$$

where α is a scalar material-dependent constant. In between these two asymptotic behaviors, the curve $F(h)$ contains all information about the pinning-field probability density $\omega(\kappa)$.

As the curve is smooth, the first and second derivatives of $F(h)$ can be evaluated at the series points x^k by finite differences with sufficient accuracy.

$$\partial_h F(x^j) = F(x^j)\frac{\Delta_2 - \Delta_1}{\Delta_1\Delta_2} + F(x^{j+1})\frac{\Delta_1}{\Delta_2\Delta_3} - F(x^{j-1})\frac{\Delta_2}{\Delta_1\Delta_3}$$

$$\partial_h^2 F(x^j) = 2\left(\frac{F(x^{j-1})}{\Delta_1\Delta_3} - \frac{F(x^j)}{\Delta_1\Delta_2} + \frac{F(x^{j+1})}{\Delta_2\Delta_3}\right)$$

with

$$\Delta_1 = x^j - x^{j-1} \quad , \quad \Delta_2 = x^{j+1} - x^j \quad , \quad \Delta_3 = x^{j+1} - x^{j-1} \tag{22}$$

and

$$\partial_h F(x^0) = 1 \quad , \quad \partial_h^2 F(x^0) = 0. \tag{23}$$

Figure 5 represents a spline interpolation of the derivative of F based on the points $\partial_h F(x^j)$. This function $\partial_h F(\kappa)$ is the primitive of $\omega(\kappa)$, (17), and hence the cumulative distribution function of the pinning field, i.e., the probability that the pinning field is lower than h. It reaches the asymptotic value one for $\kappa \approx 200$ A/m, which means that all pinning fields in the material are weaker than that value. Interestingly, the non-zero value at zero magnetic field indicates that about 10% of the microscopic regions have a zero pinning fields, i.e., behave reversibly. The cumulative distribution function of a reversible material is indeed $\partial_h F = 1$.

Experience shows that anhysteretic curves can be represented accurately by a double Langevin function[4,9]

$$J_{\text{an}}(h_r) := J_a L\left(\frac{h_r}{h_a}\right) + J_b L\left(\frac{h_r}{h_b}\right) \tag{24}$$

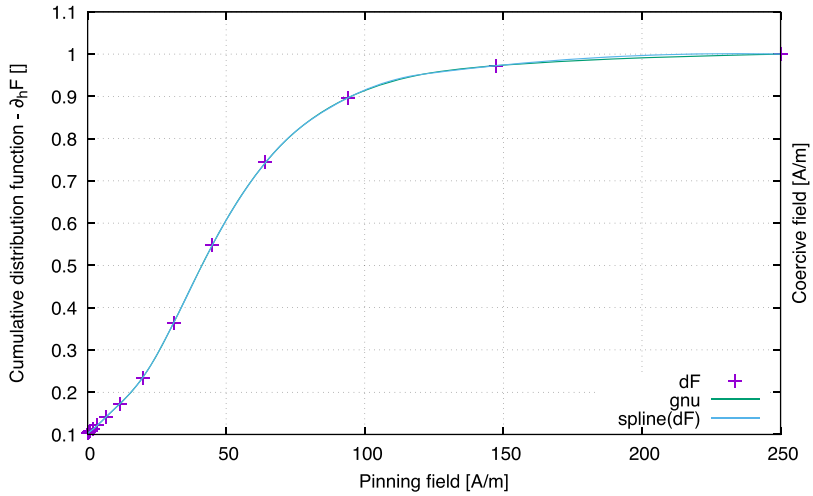

FIG. 5. Spline interpolation of the pinning field cumulative distribution function $\partial_h F(\kappa)$ based on the points $\partial_h F(x^j)$.

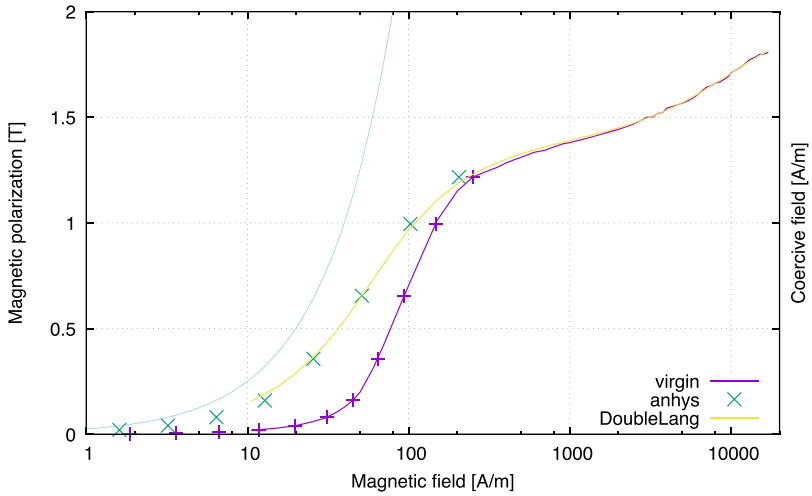

FIG. 6. Virgin curve and the identified double Langevin anhysteretic curve of the steel grade M235-35A. The asymptotic linear behavior of the anhysteretic curve at the origin is represented by the solid line.

with $L(x) = \coth x - \frac{1}{x}$. The term indexed with a b represents the magnetic polarization due to the motion of Bloch walls, whereas the term indexed with an a represents the magnetic polarization, occurring at high field intensity, that is associated with the rotation of the magnetic moments relative to their preferred easy-magnetization axis. Once the function F is known for a material, the four parameters of the double Langevin representation (24) $J_{\text{an}}(h)$ can be determined by simply matching the measured virgin curve $J_{\text{virgin}}(h)$ with $J_{\text{an}}(F(h))$. It is an evidence of the consistency of the proposed identification procedure that the curve $J_{\text{an}}(F(h))$, which combines two unrelated nonlinear function, is indeed, as expected, linear at the origin. Figure 6 depicts the anhysteretic and virgin curve for the material M235-35A.

The identification procedure relies on a set of symmetric hysteresis loops measured in unidirectional conditions. The results presented above were obtained with the standard Epstein frame protocol,[11] where the magnetic core is a stack of strips taken alternatively in the rolling direction (RD) and the transverse direction (TD), so as to average out the material's anisotropy. During the continuous measurements the magnetizing field is changed in a continuous fashion with a $\frac{\mathrm{d}B}{\mathrm{d}t}$ rate below 100mT/s, as slowly as reasonable to avoid eddy-current effects. The initial magnetization curve is determined by monotonically increasing the magnetic field strength from zero to the maximum field strength starting from the demagnetized state. The quasi-static hysteresis loop is identified by cycling the magnetic field continously from the maximum positive to the maximum negative value and back.

V. CORRELATION WITH MICROSTRUCTURAL STRUCTURE

A grain boundary is the interface between two grains, or crystallites, in a polycrystalline material. Grain boundaries are also places where defects are preferably located. If L is the grain size, the number of grains (assumed to have an aspect ratio close to 1) is $N = V/L$,[3] where V is the volume of the sample. The cumulated grain boundary surface is proportional to NL,[2] and hence to V/L. On the other hand, it is observed that coercivity is inversely proportional to the grain size. We have thus an indication that coercivity is linked with the cumulated grain boundary surface per unit volume.

The identification procedure described in the previous section has been applied to five non-oriented electrical steel grades, namely, M235-35A (3.2wt% Si), M250-35A (3.2wt% Si), M330-35A (2.4wt% Si), M330-50A (2.4wt% Si) and M400-50A (2.4wt% Si). The coercive field characteristics $h_c(h)$, the pinning field cumulative distribution functions $\partial_h F(\kappa)$, and the pinning field probability densities $\omega(\kappa)$ are depicted in Fig. 3, Fig. 7 and Fig. 8. In order to determine the grain size, the samples

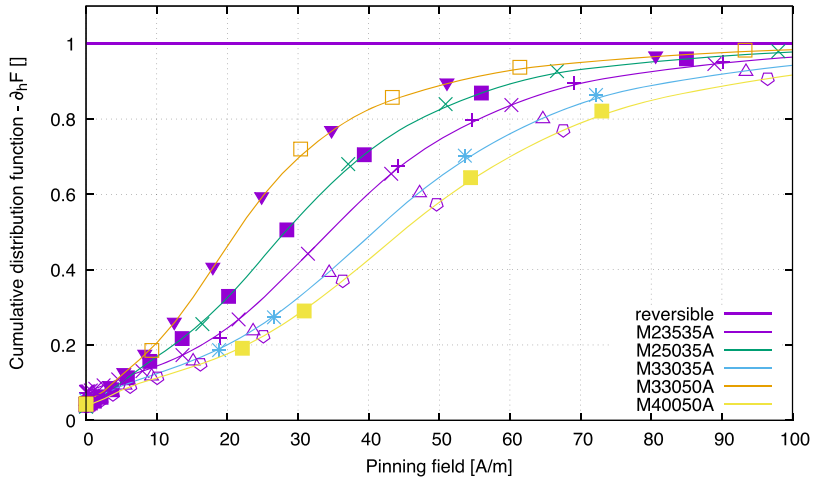

FIG. 7. Pinning field cumulative distribution function $\partial_h F(\kappa)$ for five steel grades.

were ground and polished in different layers of the RD-TD sheet plane. The determination of the grain size is performed analogous to the line intercept method and carried out along the RD and TD of the micro-section. For each spatial direction, two different micro-sections are used to determine the average grain sizes.

Each grade has its own distribution $\omega(\kappa)$, which can in principle be traced back to objective differences in the lamination thickness and in the microstructure.[10,13] For instance, M235-35A and M250-35A, have the same alloy and same thickness, but the grain size of M235-35A is 100µm, whereas the grain size of M250-35A is 109µm. The smaller average grain size of M235-35A compared to M250-35A leads to a higher coercivity, as seen in Fig. 3. This corroborates the proportionality of coercivity with the inverse of the grain size, which is also supported by the results obtained for M330-50A. The latter has the largest average grain size, 122µm, and a homogeneous grain structure. The peak in the pinning field distribution function of this grade, Fig 8, is thus narrow, because of a small standard deviation of the average grain sizes, and centered around the lowest value amog the considered materials, because of the large grain size.

A decrease in the lamination thickness also correlates with dislocation densities and has an effect on the coercive force. M330-35A has a reduced thickness and a reduced average grain size of

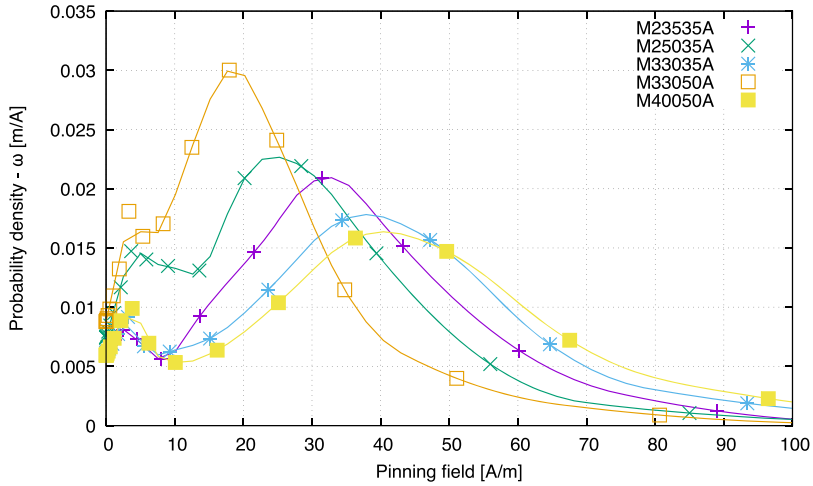

FIG. 8. Identified pinning field probability density $\omega(\kappa)$ for five steel grades. for five different steel grades.

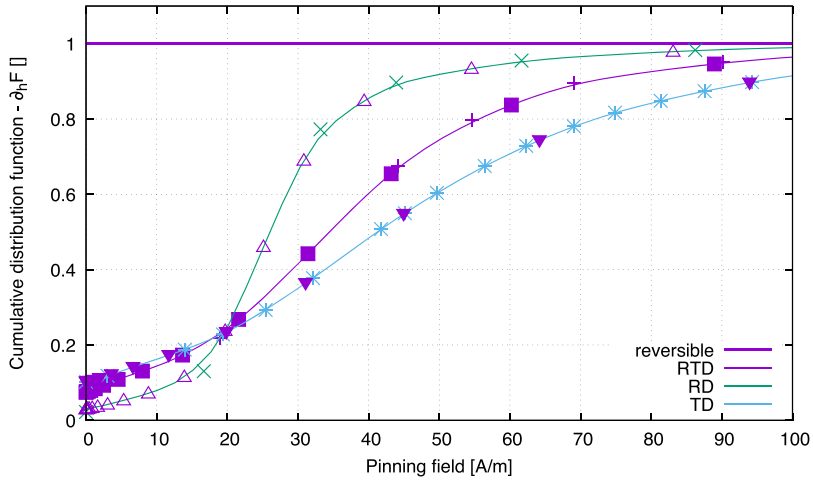

FIG. 9. Spline interpolation of the pinning field cumulative distribution function $\partial_h F(\kappa)$ based on the points $\partial_h F(x^j)$ for M235-35A in RD, TD and the standard alternate Epstein stacking (RTD).

87.5µm compared to M330-35A, with a large standard deviation due to an inhomogeneous grain structure, and with a large variation in grain sizes. This yields a flatter pinning field distribution centered around a higher field value. Finally, with the smallest average grain size of 70µm among the considered grades, M400-50A presents the higher coercivity.

Further on, it is interesting to analyze the effect of the different stacking methods, i.e., the difference in the pinning field distribution function for the RD and TD. The Epstein frame can be prepared for that purpose with all strips in RD, or all strips in TD. The results depicted in Fig. 9 and Fig. 10 are then obtained, and can be compared with those obtained with the standard alternate RD-TD-RD-TD setup (labeled RTD), for which results were shown in Fig. 7 and Fig. 8.

Due to the rolling process, grains are stretched in RD. For M235-35A, the average grain size in RD is 105µm with a small standard deviation, whereas it is about 89µm in TD, with a larger standard deviation. This is reflected in the curves presented in Fig. 10. It is so observed that the pinning field probability density $\omega(\kappa)$ is strongly influenced by the anisotropy. In combination with the orientation distribution function (ODF), which describes the magneto-crystalline texture, this can be related to the model parameters of the anisotropic vector hysteresis model.[6]

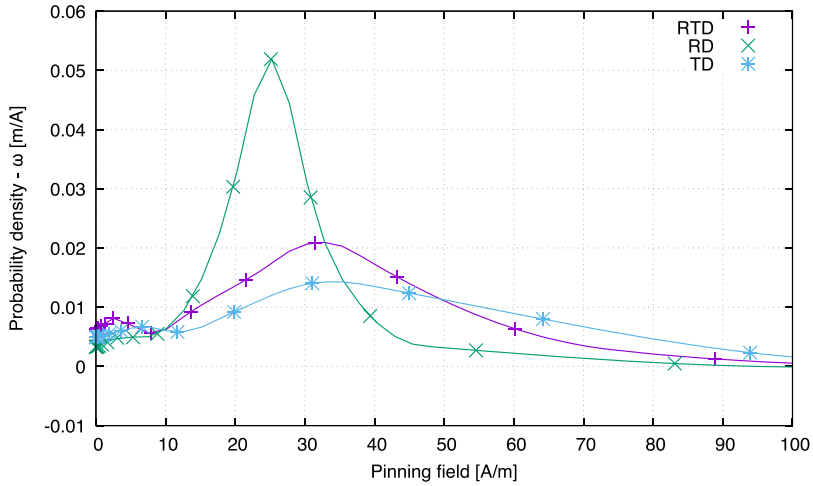

FIG. 10. Identified pinning field probability density for M235-35A and different stacking methods.

VI. CONCLUSION

On basis of an analogy between pinning field and a dry friction force, and of a multi-scale representation of microstructure, an accurate theoretical definition has been given for the probability density of pinning fields in soft ferromagnetic materials. The mathematical properties of this definition make it possible to extract, following a systematic procedure, the pinning field probability density from the coercive fields of symmetric hysteresis loops, which are easily measurable quantities. The obtained probability densities not only give insight into the microstructure of the materials, but provide also readily objective values for the free parameters of the hysteresis model, which can then be used in macroscopic finite element simulation.

[1] G. Bertotti, *Hysteresis in Magnetism* (Academic Press, New York, 1998).
[2] K. H. J. Buschow and F. R. De Boer, *Physics of Magnetism and Magnetic Materials* (Springer, US, 2003).
[3] A. Bergqvist, "Magnetic vector hysteresis model with dry friction-like pinning," Physica B **233**, 342–347 (1997).
[4] F. Henrotte, A. Nicolet, and K. Hameyer, "An energy-based vector hysteresis model for ferromagnetic materials," COMPEL **25**, 71–80 (2006).
[5] F. Henrotte and K. Hameyer, "A dynamical vector hysteresis model based on an energy approach," IEEE Trans. Magn. **42**(4), 899–902 (2006).
[6] S. Steentjes, F. Henrotte, and K. Hameyer, "Energy-based ferromagnetic material model with magnetic anisotropy," J. Magn. Magn. Mater. **425**, 20–24 (2017).
[7] A. Bergqvist, A. Lundgren, and G. Engdahl, "Experimental testing of an anisotropic vector hysteresis model," IEEE Trans. Magn. **33**(5), 4152–4154 (1997).
[8] F. Henrotte, S. Steentjes, K. Hameyer, and C. Geuzaine, "Iron loss calculation in steel laminations at high frequencies," IEEE Trans. Magn. **50**(2), 333–336 (2014).
[9] S. Steentjes, M. Petrun, G. Glehn, D. Dolinar, and K. Hameyer, "Suitability of the double Langevin function for description of anhysteretic magnetization curves in NO and GO electrical steel grades," AIP Advances **7**(5), 056013 (2017).
[10] G. Bertotti, "Connection between microstructure and magnetic properties of soft magnetic materials," J. Magn. Magn. Mater. **320**(20), 2436–2442 (2008).
[11] International Standard, Magnetic materials - Part 2: Methods of measurement of the magnetic properties of electrical steel strip and sheet by means of an Epstein frame, IEC 60404-2:1996 + A1:2008.
[12] S. Steentjes, F. Henrotte, C. Geuzaine, and K. Hameyer, "A dynamical energy-based hysteresis model for iron loss calculation in laminated cores," Int. J. Numer. Model. **27**(3), 433–443 (2013).
[13] L. Dupré, M. Sablik, R. Van Keer, and J. Melkebeek, "Modelling of microstructural effects on magnetic hysteresis properties," J. Phys. D: Appl. Phys. **35**(17) (2002).